FINITE PULSE RATCHET EFFECT OF COLD ATOMS

A Thesis
Submitted to the African University of Science and Technology
Abuja-Nigeria.

in partial fulfilment of the requirements for

MASTER DEGREE IN THEORETICAL AND APPLIED PHYSICS

By

CHUNG Gyang Davou

Supervisor:
Prof. Dr. Anatole Kenfack

AUST Abuja

March 2021

A THESIS APPROVED

BY

SUPERVISOR
……

MEMBER
……..

MEMBER
……

Abstract

The thesis presents the modelling and simulation of the rachet effect created by a spatio-temporal asymmetry potential. The potential is a coupled spatial asymmetry sin wave and a rectangular pulse train. The effective Planck's constant $\hbar$(kbar), was the indicator of the quantum nature of the system and influence the dynamic of the system. The effective kick strength Γ, the duty cycle of the pulse train τ and $\hbar$ are the key parameters that determine the possibility of directed transport in the cold atom system. The developed approach was justified by the results obtained at $\tau = 0.01$. This result approaches those of delta pulses that were already available. It was discovered that, the variation in pulse width as indicated by the values of τ influence the system dynamics. In such a way that at $\Gamma = 4.5$, with increase in τ (from 0.01 to 0.03) within the studied region of $\hbar/\pi$ = *0 to 4.9*, the absolute amplitude current at resonance decreases as kbar relatively increases. Although within a relatively lower values of kbar, the current has higher values for higher τ, before the gradual decrease as kbar increases. And it was also shown that at a fixed resonance point (kbar/pi =1.5), the ratchet current reasonably increases rapidly with increase of both τ and the kicked strength Γ.

Dedication

I dedicate this thesis to God who gave me insight, wisdom, power, and courage to complete this work.
Also, to my precious and loving parents – Rev. Gyang R. Chung and Mrs.Vou Gyang and to my siblings; Pam, Esther, Mafeng and Samuel Gyang for their support.

Acknowledgement

I am grateful to God who guides me through his Words and grand me wisdom, peace, and strength to complete my courses and thesis successfully.

Secondly, I want to appreciate my parents and siblings for their genuine love and support towards me during my program at AUST, Abuja.

I am also deeply grateful to Prof. Anatole Kenfack for all his concerns and support during my studies and Thesis. You were always accessible and ready to listen to any complain.

My gratitude also goes to all the staffs and students at African University of Science and Technology (AUST), Abuja, and to all my friends. My sincere appreciation goes to Dr. Akosa for all his tutoring and advice and to my colleagues in Theoretical Physics: Dennis Tonui, Odeke, Kabir and Fummi. And to the AUST Physics Alumni for all their support.

CONTENTS

Chapter 1: Introduction

1.1 Directed Transport . . . . . .

1.2 Statement of the Problem . . . . . .

1.3 Overview of the Thesis . . . . . .

Chapter 2: Literature Review

2.1 Ratchets Definition . . . . . .

2.2 Feynman ratchets in detail . . . . . .

2.3 Directed transport. . . . . .

2.4 Some Applications of Ratchet Effects . . . . .

2.5 Common types of Symmetry in ratchet systems . . . .

2.6 Occurrence and classification of Resonance . . . .

2.7 Modes of Hamiltonian setup in ratchet studies . . . .

2.8 Some Flashing Ratchet Cold Atom Systems

Chapter 3: Methodology

3.1 The Split-Operator Method . . . . . .

3.2 Finite Pulse Train . . . . . .

3.3 Model of Finite Pulsed cold Atom . . . . .

3.4 Wave Function, Current and Energy . . . . .

Chapter 4: Results and Discussion

4.1 Duty Cycle of Pulse Train . . . . . .

4.2 Correspondence of Finite Pulse Train Solutions to Delta Kicks at $\tau = 0.01$

4.3 Current and Energy Growth at Resonance Points. . . .

4.4 Finite Pulse Effect with Kbar ($\hbar$) . . . . .

4.5 Finite Pulse Effect with $\hbar = 1.5\pi$ at Various Potential Strength Γ .

4.6 Finite Pulse Effect for Various Potential Strength Γ and $\hbar/\pi$ (kbar/pi) Variation at $\tau = 0.01$ . . . . . .

Chapter 5: Conclusion and Outlook

5.1 Conclusion . . . . . .

5.2 Outlook . . . . . .

Reference . . . . . .

CHAPTER 1
INTRODUCTION

1.1 Directed Transport

With the motivation to understand directed transport on a molecular scale,[1] the so-called "Brownian motors" became an area of research interest. Originally proposed by Feynman[2]. Ratchet effect is the possibility to obtain directed motion without bias (time-average equal to zero) in periodic systems with broken symmetries[2]. However, the second law of thermodynamics prohibits this effect in systems at equilibrium[3]. Hence, directed transport of particles become possible, when relevant spatiotemporal symmetries are broken, and particles are driven out of equilibrium[2],[4]. This effect found many applications. Such as the physics modelling of molecular motors in biological systems, molecular switches, particle selectors, development of nano devices[5][6][7] in which ratchet effect that is artificially created and serves as electron pump [2]etc.

This effect has transcended from the earlier focused classical regime[8] to quantum regime[9][10][11][12]. Thereby opening an avenue for exploring quantum phenomena. As progress [13][7]are being made to develop devices that are based on this effect[8]. Detailed discussion of directed transport is provided in chapter 2.

1.2 Statement of The Problem

In exploring quantum phenomena and other possibilities that this effect introduced. Infinite (delta-kicked) pulse ratchet system had been developed and studied. However, practically created ratchet potential from superposition of optical beams are finite pulses. Hence, a need to develop and study a more realistic ratchet effect of cold atoms with finite pulse emerges.

This work aimed at developing an optically finite pulse cold atom system and the associated computational code. After which, the effect of the finite pulse will be explored.

1.3 Overview of The Thesis.

Chapter two reviews the previous work and progress made in ratchet and related research. Chapter three gives the detailed development of our system. It started with the discussion on the split operator method that was employed to solve the wave packet dynamic of the

system. It was followed by a discussion on the finite pulse train development from Fourier series. After which the Hamiltonian was developed for the cold atom dynamics. The equations for the computation of the wavefunction, current and energy were then obtained. Results obtained from the numerical solution were presented and discussed in chapter four, followed by the conclusion and outlook in chapter five.

CHAPTER 2
LITERATURE REVIEW

The motion of liquid droplets on hot metallic asymmetrical surfaces, the biological molecular transport in systems such as proteins and bacteria, and the Feynman-Smoluchowski Ratchet Device[5], [8]. Are some common examples of directed transport from chaos, in this fascinating field of research. Hence, this chapter presents several aspects of the ratchet effect and the progresses made in this interesting field.

2.1 Ratchets Definition

Questioning certain possibilities in science is often a source of inspiration for many. One of such question is, “Can one extract useful work from thermal fluctuations?”[5]. This single question became a source of inspiration for many individuals that lead to gedanken experiments to actual designs of perpetual motion machines. However, the consequences of the Second Law of Thermodynamics prove itself more powerful to the ideas they proposed, and none of their design come to fruition. None the less, Smoluchowski and Feynman [14]were part of such community but with different intention. They made such a design, only with the motivation of showing that we could never derived work at thermal equilibrium. Their machine as seen in Fig. 2.1. However, when operating out of equilibrium can rectify fluctuations. Hence, one can easily define a ratchet as a system exhibiting directed transport away from equilibrium due to zero-mean fluctuations. A very similar device to a ratchet is the Brownian motor. In that it rectifies fluctuations. The difference between the two is that Brownian motor operates solemnly due thermal zero mean fluctuations. While a ratchet can operate even in a completely Hamiltonian systems with only a zero mean external driving force. It should be noted that for both ratchets and Brownian motors, the Second Law of thermodynamic is accounted for by the devices consuming energy to stay away from equilibrium.

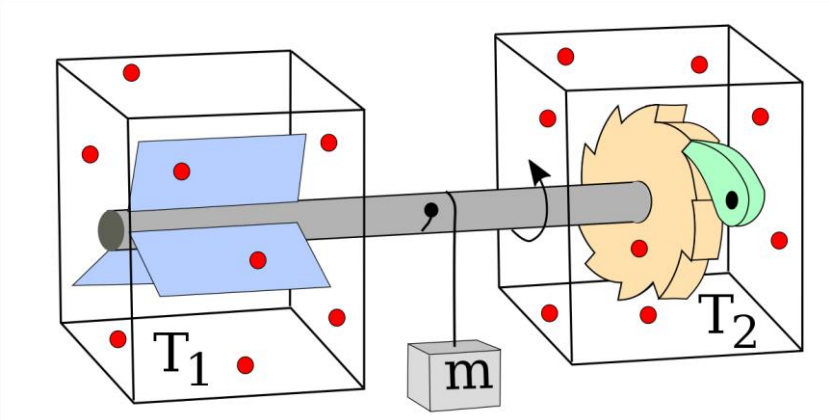

Fig. 2.1: Carton of Feynman-Smoluchowski ratchet device [14]. The ratchet and-pawl device in box 2 with particles at temperature T_2 rotates due to thermal fluctuations of particles in box 1 with temperature T_1. The pawl is developed to rectify the unbiased fluctuations in 1, resulting in single direction rotation and the possibility of executing work on a mass m connected to the axle.

2.2 Feynman ratchets in detail

Feynman extended a thought experiment of Smoluchowski [3] on the possibility of deriving energy from microscopic fluctuations. With a well-known ratchet system often referred to as the Feynman ratchet. The basic idea was to employ a device with a single axle. With on one side a ratchet and-pawl, a cog with asymmetric teeth and a lever. While on the other side having large fins. Because of Brownian motion the surrounding fluid randomly pushes on the fins, while the pawl enable the axle to rotate only in a single direction. On first look, it seems plausible that this device, in Fig. 2.1, can lift a mass attached to the axle and thereby accomplish useful work. However, Feynman showed that if the whole system is at thermal equilibrium no useful work can be derived from the Brownian motion of the gas. Simply because the pawl, microscopic in size itself to allow any rotation of the axle, experiences Brownian motion as well. When the pawl is lifted by a thermal fluctuation the ratchet can move in the direction that is otherwise blocked. The net result is that the rotation rates to the left and the right are exactly equal. If this were not the case the pawl would be a classical example of a Maxwell's demon. But extraction of work is possible if the temperature of the gas surrounding the fins is larger than that surrounding the ratchet. Though in that case the Second Law does not apply, and the system is simply a microscopic heat engine.

2.3 Directed transport.

The ratchets of Feynman and Brillouin rectifier were designed to show the effect of the Second Law, and to paradoxically not produce work at equilibrium.

One can however turn this around and start thinking about designing devices that operate away from equilibrium and do useful work without violating the Second Law. An interesting step in this direction was made by Tsong and Astumian[15], who in 1986 proposed the flashing ratchet as the mechanism on which some classes of molecular motors operate. Molecular motors are proteins that stays in a noisy environment in the biological body, and transform random 'kicks', experienced when transforming ATP to ADP, in directed motion with the support of a spatially asymmetric potential. This enables them to transport certain load around the body. Providing insight into the principle of operation of molecular motors was one of the reasons for the increase in interest and progress in ratchets development. In 1993, Magnasco [16] gave a broader significance of ratchets, when he showed that directed motion is a generic character of a system out of equilibrium and with broken symmetry. As a result, many theoretical work [17], [18] and experimental demonstrations of ratchets with colloidal particles [18] and optically trapped beads [19] were performed. And in a few distance of time, new technological applications emerged on the horizon.

2.4 Some Applications of Ratchet Effects

Ratchet effect found many near time applications. One of such is the use of ratchets principle in particle separation devices. In such application development, It has already been shown that particles with different features like size or mass can be influence to move in opposite directions[18]. it has already made it possible to separate phospholipid molecules[20] . The principle can easily be extended to many other types of molecules even in their local environment, something that is very difficult to accomplish any other way. Other applications for ratchets include electron pumps[21], voltage rectification across Josephson junctions, vortex density control in superconductors[22] and nanoscale machinery [23]. They are also of interest in theoretical non-equilibrium thermodynamics discussions. Which encompasses both classical and quantum[24] transport phenomena to the test of fluctuation theorems [25].

2.5 Common types of Symmetry in ratchet systems:

Since the possibility of observing directed transport depends on the asymmetry of the system[6]. Generally, symmetry analysis [12][11] is employed to determine the symmetry of the system which has the potential to prevent directed transport[7]. Although depending on the kind of potential available, there are two types of symmetries that often surface. The shift (Translational) and the time-reversal symmetry[3][26].

The shift symmetry characterized to invariance under the translational transformation $(r, p, t) \rightarrow (-r, -p, t + T/2)$.

Where T is the period of the drive.

While time-reversal symmetry corresponds to invariance under the transformation

$(r, p, t) \rightarrow (r, -p, -t)$.

The kind of potential taken for our system, the shift symmetry is broken by the summation of sinusoidal functions of different amplitudes and frequency[2], [27], [28]. Hence directed transport can be produced.

It should be noted that the presents of these two symmetries in a potential does not completely imply that directed transport would not occur, as other mechanism can induce directed motion. Gummer's [5] shows that for a system with symmetric driving and a symmetric potential, directed motion can be caused by dissipation induced breaking of time-reversal symmetry. Which happens in the limit of small driving amplitude and high dissipation.

2.6 Occurrence and classification of Resonance:

Ballistic rather than diffusive current and energy growth [1], [2]often observed at quantum resonance are the indicators of ratchet effects in a Quantum system. They emerged when the flashing frequency w is commensurate with the recoil frequency w_R.[2], [29] It is related to the arithmetic nature of the effective Planck constant $\hbar$ of the kicked system, particularly occurring if.

$$\hbar = \frac{4\pi r}{s} \quad . \quad . \quad . \quad . \quad . \quad . \quad . \quad . \quad . \quad (2.1)$$

Where r, s are mutually prime integers. low-order quantum resonance (LOQR) and high-order quantum resonance (HOQR) are classified based on the value of s. where cases with small s are called LOQR and those with large s values are HOQR.

2.7 Modes of Hamiltonian setup in ratchet studies

There are two often used Hamiltonian setups in both classical and quantum ratchet systems[30]. They are the flashing[2], [29] and rocking mode[1], [10]. Flashing ratchets are realized with multiplicative driven potentials, $V(x) * F(t)$. While rocking ratchets are characterized by periodically tilted potentials, often obtained by summing of position and time dependent potentials $U(x,t) + V(x) + F(t)$. Hence in rocking mode of operation the forcing term enters additively, whereas it is of multiplicative character for the flashing mode. Consequently, the two setups are members of different dynamical symmetry groups[30]. Specifically, the rocking ratchet can be obtained with a single harmonic potential. And a flashing ratchet required a potential with a minimum of two spatial harmonics[7], [30].

2.8 Some Flashing Ratchet Cold Atom Systems

Cold atoms systems under the influence of different kinds of potentials created optically have been studied. Some have even been explored experimentally [13].

The theoretical exploration of ratchet effects in the flashing mode earlier accomplished by Emil et al[27] with the observation of LOQR. Was further studied and the emergence of HOQR was observed by Kenfack et al [2]. Chen et al [28]extended this Hamiltonian to account for double kicks, where they observed the emergence of HOQR and some resonance at points not earlier seen. A recap of their equations is given in equation 2.2 [2], [27]and 2.3[28].

$$i\tilde{\hbar}\frac{\partial\psi}{\partial t} = -\frac{\tilde{\hbar}^2}{2}\frac{\partial^2\psi}{\partial x^2} + v(x)\sum_{l=0}^{\infty}\delta(t-\iota)\psi \quad . \quad . \quad . \quad . \quad . \quad (2.2)$$

$$i\tilde{\hbar}\frac{\partial\psi}{\partial t} = -\frac{\tilde{\hbar}^2}{2}\frac{\partial^2\psi}{\partial x^2} + \sum_{l=0}^{\infty}[K_1 v_1(x)\delta(t-2\mathrm{n}) + K_2 v_2(x)\delta(t-2\mathrm{n}-\tau)]\psi \quad . \quad (2.3)$$

Where $v(x) = sinx + \alpha sin(2x)$, $v_1(x) = sinx$, $v_2(x) = sin(2x)$, K_1 and K_2 are the strengths of two potentials, τ is a time parameter with $0 \leq \tau < 2$, and n takes integer values. For detail discussion of those equations, refer to the corresponding papers.

Their results, however, have been limited to delta kicks. Exploring this system with finite pulse become something of interest as it indicates the possibility of taken us closer to what will be easily observed experimentally.

Although, a possible reason for staying at such limit is the complexity that it may introduced [27]. However, the inclusion of finite pulse has been successfully implemented in some systems earlier. Like the quantum kicked rotor[10], [29]. Those work will form a guide in the development and implementation of finite pulse in the flashing ratchet system of cold atoms. The system is captured in equation (2.4) with detailed discussion in chapter 3.

$$i\hbar\frac{\partial\psi}{\partial t} = -\frac{\hbar^2}{2}\frac{\partial^2\psi}{\partial x^2} + v(x)\sum_{n=0}^{n} F(t-nT)\psi \quad . \quad . \quad . \quad . \quad . \quad (2.4)$$

This work desire to show how the finite width and the corresponding modification of the potential coefficient that unavoidably arises in a real experiment[1], [2], [29] due to the finite temporal width of the kicks can also be exploited to produce a strongly asymmetric system and resonances. This will be achieved by solving and exploring equation 2.5. with expectation of resonance and the possibility of resonance in points not earlier observed.

CHAPTER 3
METHODOLOGY

Here, the underpinning methods that lead to the results obtained in this work are discussed. And it is the basis on which our discussions of results lie on and determine the regime of the applicability of our results.

3.1 The Split-Operator (Split-Step) Method

Quantum wave-packet dynamics is the evolution of the spatial distribution of a quantum particle [31]. And it forms an important part of the simulation of cold atom dynamics. Because the information about the system is contained in the wave-packet and its evolution in time.

The Split-Operator Method is a general-purpose technique to solve a compatible time-dependent Schrödinger equation (TDSE) [31]. It is of particular interest for quantum particle interacting with a time-dependent or time and position-dependent potential. It has been successfully employed in many different settings. Such as the simulation of high-power laser-matter interactions[32]. It can also be employed in equations, like the Gross-Pitaevskii [33] and Dirac equations [34], [35].

It is a spectral method that was developed by Feit and Fleck in the 1980's[4]. And the description of the method follows by considering the time dependent Schrödinger equation (TDSE),

$$i\hbar\frac{\partial}{\partial t}\psi(t) = \widehat{H}\psi(t) \quad . \quad . \quad . \quad . \quad . \quad . \quad . \quad . \quad (1)$$

With $\psi(t)$ been the wavefunction and $\widehat{H}$ the Hamiltonian for the dynamic of a particle under the influence of an external time-dependent potential $V(t)$,

$$\widehat{H} = \widehat{K} + \widehat{V} = \frac{\hat{P}^2}{2m} + \widehat{V}(t) \quad . \quad . \quad . \quad . \quad . \quad . \quad . \quad (2)$$

Where the kinetic, potential energy and momentum operators, are $\widehat{K}$, $\widehat{V}$ and $\hat{P}$ respectively, with m been the mass of the particle.

Given that $\widehat{U}$ is the time evolution operator. The formal solution to equation (1) is given by $\widehat{U}$. Hence.

$$i\hbar\frac{\partial}{\partial t}\hat{U} = \hat{H}\hat{U} \quad . \quad . \quad . \quad . \quad . \quad . \quad . \quad . \quad (3)$$

In general, the solution at any time t given an initial wave function at time t_0, $\psi(t_0)$ is obtained as

$$\psi(t) = \hat{U}(t, t_0)\psi(t_0) \quad . \quad . \quad . \quad . \quad . \quad . \quad . \quad (4)$$

With a time-dependent Hamiltonian $\hat{H}(t)$, putting (4) into (1), one obtained.

$$\hat{U}(t, t_0) = \hat{T}\exp\left[-\frac{i}{\hbar}\int_{t_0}^{t}\hat{H}(t')dt'\right] = \hat{T}\exp\left[-\frac{i}{\hbar}\int_{t_0}^{t}\left[\hat{K} + \hat{V}(t')\right]dt'\right]. \quad . \quad (5)$$

$\hat{T}$ is the time-ordering operator that ensures that Hamiltonian is applied to the wave function in order of increasing time, as in general the Hamiltonian does not commute with itself at a different time, i.e., $\left[\hat{H}(t), \hat{H}(t')\right] \neq 0$.

By considering a small-time increment Δt, $\hat{T}$ is negligible and one approximate the short-time evolution operator as

$$\hat{U}(t + \Delta t, t) = \exp\left[-\frac{i}{\hbar}\int_{t}^{t+\Delta t}\left[\hat{K} + \hat{V}(t')\right]dt'\right] \quad . \quad . \quad . \quad . \quad (6)$$

The form of the potential is not limited to time-dependent but can also have a spatial dependence component, i.e $\hat{V} \equiv \hat{V}(x, t')$. Here, $\hat{K}$ and $\hat{V}$ do not commute. Hence, Baker-Campbell-Hausdorff formula, given in equation (7) for the exponential [4] of the operator is applied.

$$\exp\{t\left[\hat{A} + \hat{B}\right]\} = \exp\left(t\,\hat{A}\right)\exp\left(t\,\hat{B}\right)\exp\left(-\frac{t^2}{2!}\left[\hat{A}, \hat{B}\right]\right)\exp\left(-\frac{t^3}{3!}(2\left[\hat{B}, \left[\hat{A}, \hat{B}\right]\right] + \left[\hat{A}, \left[\hat{A}, \hat{B}\right]\right]\right) \quad . \quad . \quad . \quad . \quad . \quad . \quad . \quad . \quad . \quad (7)$$

With t = 1. Considering first order approximation of equation (7), allows the approximation of the evolution operator with minimal error,

$$\hat{U}(t + \Delta t, t) = \exp\left[-\frac{i\Delta t}{2\hbar}\hat{K}\right]\exp\left[-\frac{i}{\hbar}\int_{t}^{t+\Delta t}\hat{V}(t')dt'\right]\exp\left[-\frac{i\Delta t}{2\hbar}\hat{K}\right] + O(\Delta t^3). \quad (8)$$

And the potential can be integrated using the midpoint formula,

$$\int_{t}^{t+\Delta t} f(t')dt' = f(t + \Delta t/2)\Delta t + O(\Delta t^3) \quad . \quad . \quad . \quad . \quad . \quad (9)$$

Hence.

$$\widehat{U}(t+\Delta t,t)=\exp\left[-\frac{i\Delta t}{2\hbar}\widehat{K}\right]\exp\left[-\frac{i\Delta t}{\hbar}\widehat{V}\left(t+\frac{\Delta t}{2}\right)\right]\exp\left[-\frac{i\Delta t}{2\hbar}\widehat{K}\right] \quad . \quad . \quad (10)$$

Where $O(\Delta t^3)$, is the associated commutation error. It can be made acceptably small if Δt is chosen sufficiently small. The choice of the order of the operators $\widehat{K}$ and $\widehat{V}(t')$ in the above equations is arbitrary. It is often based on how fast one can get the solution.

Equation (10) implies calculating exponential $\widehat{K}$ and $\widehat{V}(t')$ which is trivial because the operators are diagonal matrix in momentum space and spatial configuration, respectively. By employing Fourier transform $\mathcal{F}$ and its inverse $\mathcal{F}^{-1}$, one can move from one space to another as shown in equation (11). Where the kinetic energy was shifted from momentum space to spatial configuration.

$$\exp\left[-\frac{i\Delta t}{2\hbar}\widehat{K}(\boldsymbol{X})\right]\psi(\boldsymbol{X})=\mathcal{F}^{-1}\exp\left[-\frac{i\Delta t}{2\hbar}\widehat{K}(\boldsymbol{P})\right]\mathcal{F}\psi(\boldsymbol{X}) \; . \quad . \quad . \quad (11)$$

with $\widehat{K}(\boldsymbol{P})=\frac{\boldsymbol{P^2}}{2m}$ and $\widehat{K}(\boldsymbol{X})=-\frac{\hbar^2}{2m}\nabla^{\boldsymbol{2}}$

The implementation of Split operator method can then be summarized in an algorithm form as:

First Approach:

$t_j = t_0 + j\Delta t, \;\; j = 0 \ldots n-1$

Initialize $\psi(\boldsymbol{X}, t=0)$

For j ⟵ 1 to $n-1$ **do**

$\psi(\boldsymbol{X})$ ⟵ Multiply $\psi(\boldsymbol{X})$ by $\exp\left[-\frac{i\Delta t}{2\hbar}\widehat{V}(\boldsymbol{X},t)\right]$

$\tilde{\psi}(\boldsymbol{P})$ ⟵ $\mathcal{F}\psi(\boldsymbol{X})$

$\tilde{\psi}(\boldsymbol{P})$ ⟵ Multiply $\tilde{\psi}(\boldsymbol{P})$ by $\exp\left[-\frac{i\Delta t}{\hbar}\frac{\boldsymbol{P}^2}{2m}\right]$

$\psi(\boldsymbol{X})$ ⟵ $\mathcal{F}^{-1}\tilde{\psi}(\boldsymbol{P})$

$\psi(\boldsymbol{X})$ ⟵ Multiply $\psi(\boldsymbol{X})$ by $\exp\left[-\frac{i\Delta t}{2\hbar}\widehat{V}(\boldsymbol{X},t)\right]$

Calculate observables $\langle\widetilde{\boldsymbol{A}}\rangle = \langle\psi(\boldsymbol{X})|\widetilde{\boldsymbol{A}}|\psi(\boldsymbol{X})\rangle$

End

Second Approach:

$t_j = t_0 + j\Delta t, \quad j = 0 \ldots n-1$

Initialize $\psi(\boldsymbol{X}, t = 0)$

For j ⟵ 1 to $n-1$ **do**

$\tilde{\psi}(\boldsymbol{P}) \longleftarrow \mathcal{F}\psi(\boldsymbol{X})$

$\tilde{\psi}(\boldsymbol{P}) \longleftarrow$ Multiply $\tilde{\psi}(\boldsymbol{P})$ by $\exp\left[-\frac{i\Delta t}{2\hbar}\frac{\boldsymbol{P}^2}{2m}\right]$

$\psi(\boldsymbol{X}) \longleftarrow \mathcal{F}^{-1}\tilde{\psi}(\boldsymbol{P})$

$\psi(\boldsymbol{X}) \longleftarrow$ Multiply $\psi(\boldsymbol{X})$ by $\exp\left[-\frac{i\Delta t}{\hbar}\hat{V}(\boldsymbol{X}, t)\right]$

$\tilde{\psi}(\boldsymbol{P}) \longleftarrow \mathcal{F}\psi(\boldsymbol{X})$

$\tilde{\psi}(\boldsymbol{P}) \longleftarrow$ Multiply $\tilde{\psi}(\boldsymbol{P})$ by $\exp\left[-\frac{i\Delta t}{2\hbar}\frac{\boldsymbol{P}^2}{2m}\right]$

$\psi(\boldsymbol{X}) \longleftarrow \mathcal{F}^{-1}\tilde{\psi}(\boldsymbol{P})$

Calculate observables $\langle\widetilde{\boldsymbol{A}}\rangle = \langle\psi(\boldsymbol{X})|\widetilde{\boldsymbol{A}}|\psi(\boldsymbol{X})\rangle$

End

3.2 Finite Pulse Train

A pulse is a single signal whose amplitude deviates from zero for a short period of time[36]. And pulse train is when there is more than one pulse. Fig 3.1 shows a sample of pulse train and some parts.

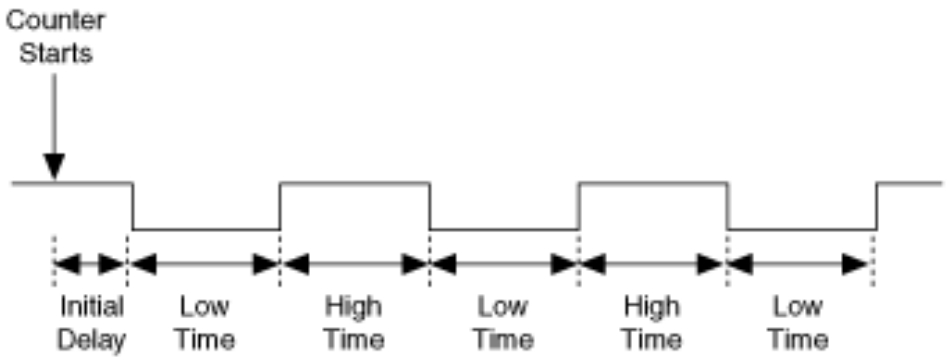

Fig. 3.1: Parts of a pulse train.

In general, pulse train have an Initial delay, Low time, and High time (Pulse width, T_1)[36]. The time taken for the output to remains at the idle state before generating the pulse is the Initial delay. While the time taken when the pulse is at a high level is the High Time and the time taken for it to be at low level is the Low Time as seen in Fig. 3.1.

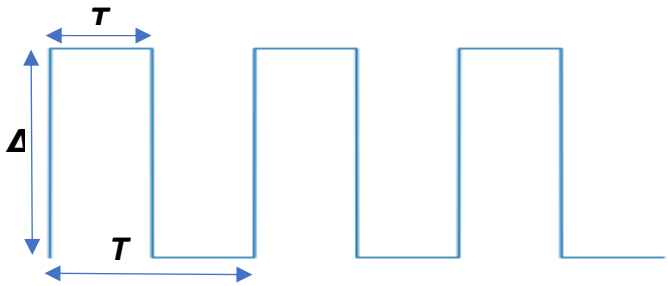

Fig. 3.2: Pulse train with amplitude A, pulse width T_1 and period T.

The sum of the high and low time is the period T, and reciprocal of the period is the frequency of the pulse. The maximum heigh of the pulse from zero is the amplitude (A) while the Duty Cycle τ, is the ratio of high time to the pulse period as given in equation (14).

$$\text{Duty Cycle } (\tau) = \frac{\text{High Time } (T_1)}{\text{Pulse Period } (T)} \quad . \quad . \quad . \quad . \quad . \quad . \quad (14)$$

Hence, a duty cycle greater than 0.5 indicates that the high time is greater than the low time and for values less than 0.5 indicates that the low time is greater than the high time.

Consider the rectangular Pulse train given by equation (15) and pictorially represented in Fig. 3.3.

$$X(t) = \begin{cases} X_1 & 0 \le t \le T_1 \\ 0 & T_1 < t < T \end{cases} \quad . \quad . \quad . \quad . \quad . \quad . \quad . \quad (15)$$

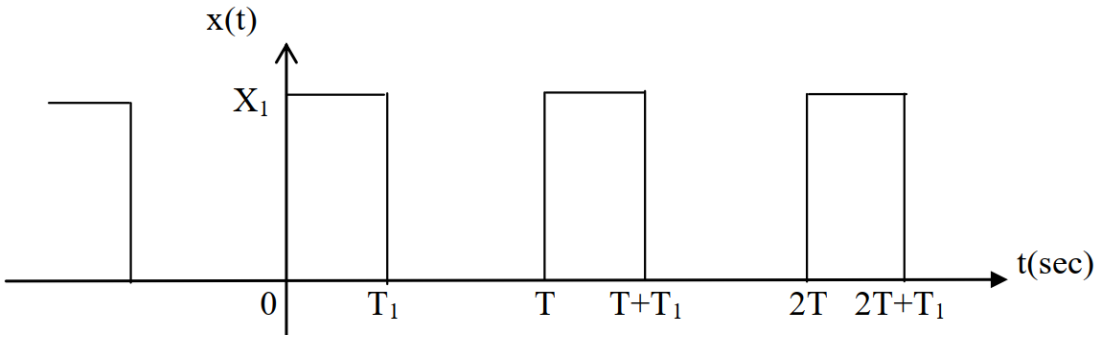

Fig. 3.3: Rectangular Pulse train signal of period T, pulse width T_1.

To be able to couple the pulse of equation (15) to the problem under study, it is more feasible when the pulse is represented in Fourier series. The Fourier series is given in its general form in equation (16)

Fourier series is a tool for writing a periodic function $X(t)$ of period T, as a summation of sines and cosines, with frequencies that are integer k, multiples of the fundamental frequency, $\omega_1 = 2\pi f_1 = \frac{2\pi}{T}\ rad/s.$ And $\omega_k = k2\pi f_1 = k\omega_1 = \frac{2\pi k}{T}\ rad/s$ is the kth frequency component.

$$X(t) = \frac{A_0}{2} + \sum_{k=1}^{\infty}(A_k cosk\omega_1 t + B_k sink\omega_1 t) \quad . \quad . \quad . \quad . \quad (16)$$

$\frac{A_0}{2}$ is the amplitude of the zero-frequency component. A_k, B_k are the Fourier coefficients. These parameters for equation (15) are:

$$\frac{A_0}{2} = \frac{X_1 T_1}{T},\ A_k = \frac{X_1}{k\pi}\left[\sin\frac{2\pi k T_1}{T}\right] \text{ and } B_k = \frac{X_1}{k\pi}\left[1 - \cos\frac{2\pi k T_1}{T}\right] \quad . \quad . \quad . \quad (17)$$

Putting equation (17) into (16), one obtains the Fourier representation of (15) and is depicted in Fig. 3.4. With amplitude of 2, period 1, pulse-width 0.5 and duty cycle of 0.5.

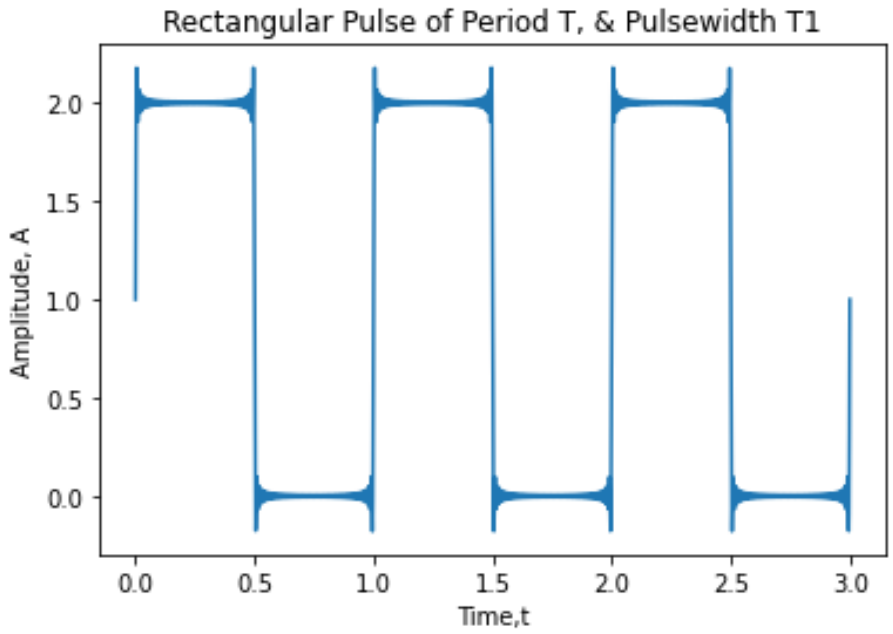

Fig. 3.4. Plot of Fourier transformed rectangular pulse.

It can be observed that the approximation is poor close to the discontinuity. This is known as the Gibbs phenomenon. It comes because of approximating a discontinuous function with a finite series of continuous functions. This problem was overcome in the computation by employing a condition that assigned the amplitude A value to X(t), so long as the result of the Fourier representation is 0.5 times the amplitude and above such value in the high time region. Hence, the pulse train becomes a perfect rectangular pulse that is shown in Fig. 3.5.

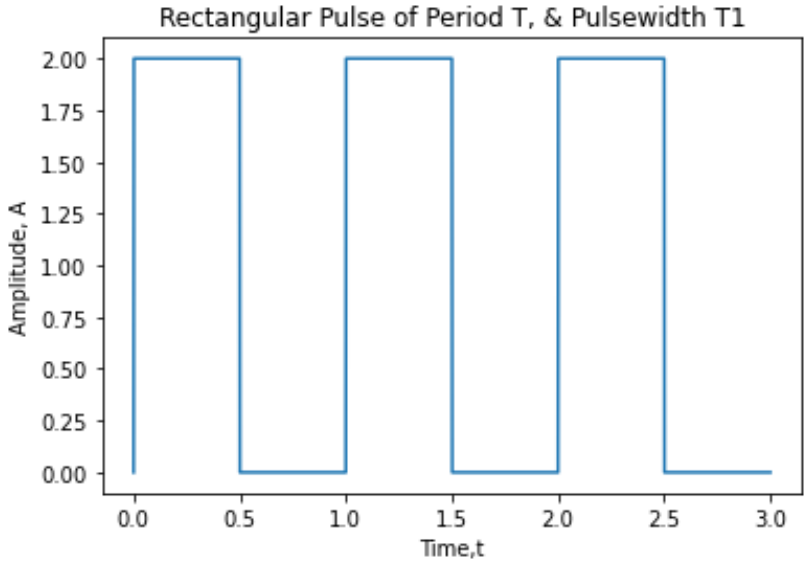

Fig. 3.5: Developed rectangular pulse train.

3.3 Model of Finite Pulsed Cold Atom

We consider a system of cold atom that is under the influence of an asymmetric optical potential $v(x)$

$$v(x) = V_0(sin2k_lx + \alpha sin4k_lx) \quad . \quad . \quad . \quad . \quad . \quad . \quad (17)$$

Where the parameter α controls the skewness of the periodic potential and is the origin of the ratchet effect. It takes values in the interval $0 \leq \alpha \leq 1$, such that for α in the range of 0 to 0.5, potential lean to the left while for the remaining range the potential lean to the right[2]. The potential become symmetric for value of $\alpha = 0$. V_0 is the amplitude of the potential. Fig. 3.6 portrait a carton of such a potential with trapped cold atoms.

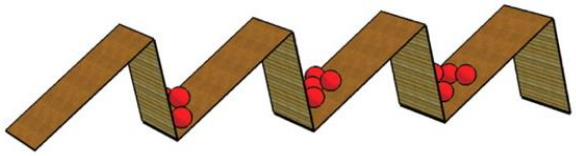

Fig. 3.6: A sinusoidal asymmetrical optical potential image

The cold atom is also moderated by a periodic-time dependent driving force $X(t)$ that is coupled with the asymmetric potential $v(x)$. Here $X(t)$ is a finite pulse train that periodically kick the system.

$$X(t) = \sum_{n=0}^{n=N} F(t-nT) = \begin{cases} X_1 & 0 \leq t \leq T_1 \\ 0 & T_1 < t < T \end{cases} \quad . \quad . \quad . \quad . \quad (18)$$

$$X(t) = \sum_{n=0}^{n=N} F(t-nT) = \frac{X_1T_1}{T} + \sum_{k=1}^{\infty} \frac{X_1}{k\pi} [\sin \frac{2\pi kT_1}{T} cosk\omega_1 t +$$

$$(1 - \cos \frac{2\pi kT_1}{T}) sink\omega_1 t] \quad . \quad . \quad . \quad (19)$$

Hence, the total Hamiltonian can be written as

$$H = \frac{P^2}{2m} + V(x)X(t) \equiv \frac{P^2}{2m} + V(x) \sum_{n=0}^{n=N} F(t-nT) \quad . \quad . \quad . \quad (20)$$

$$H = \frac{P^2}{2m} + V_0(sin2k_lx + \alpha sin4k_lx)\, X(t) \quad . \quad . \quad . \quad . \quad . \quad (21)$$

Where T is the flashing period of the light that is being switched on and off periodically. With $\omega = \frac{1}{T}$. Here, scaled units are used. Therefore, both the spatial length and the temporal T periods were set to unity. And n is an integer that counts the number of kicks.

A carton portrait of the behaviour of the system of cold atoms subject to the Hamiltonian in equation (21) is in given in Fig. 3.7. Here, the ON and OFF states are regulated by $X(t)$.

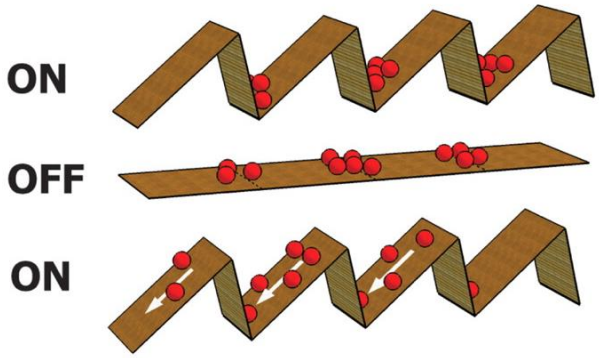

Fig. 3.7: Carton portrait of the behavior of the coupled optical potential

To transform equation (21) to dimensionless equation, one defined some new variables as

$$x' = 2K_l x \quad . \quad . \quad . \quad . \quad . \quad . \quad . \quad . \quad . \quad (22a)$$

$$P' = \frac{2K_l}{mw} P \quad . \quad . \quad . \quad . \quad . \quad . \quad . \quad . \quad . \quad (22b)$$

$$t' = wt = \frac{t}{T} \quad . \quad . \quad . \quad . \quad . \quad . \quad . \quad . \quad . \quad (22c)$$

Putting equation (22) into equation (21), one obtains

$$\frac{4K_l^2}{mw^2} H = H' = \frac{P'^2}{2} + \frac{V_0 4K_l^2}{mw^2}(sinx' + \alpha sin2x')\, X(Tt') \quad . \quad . \quad . \quad (23)$$

The resolved Hamiltonian is now $H' = \frac{4K_l^2}{mw^2} H$. Therefore H' is.

$$H' = \frac{P'^2}{2} + KX_1(sinx' + \alpha sin2x')\{\frac{T_1}{T} + \sum_{k=1}^{\infty} \frac{1}{k\pi}[\sin\frac{2\pi kT_1}{T} cosk\omega_1 Tt' +$$
$$(1 - \cos\frac{2\pi kT_1}{T}) sink\omega_1 Tt']\} \quad .$$

$$H' = \frac{P'^2}{2} + K'(sinx' + \alpha sin2x')\{1 + \frac{1}{\tau\pi}\sum_{k=1}^{\infty}\frac{1}{k}[\sin 2\pi k\tau\, cosk\omega_1 Tt' + (1 - \cos 2\pi k\tau) sink\omega_1 Tt']\} \quad . \quad . \quad . \quad . \quad . \quad . \quad (24)$$

Where $K = \frac{4K_l^2 V_0}{mw^2}$, $K' = \tau K X_1$, X_1 is the pulse amplitude and $\tau = \frac{T_1}{T}$ is the duty cycle of the temporal pulse potential. $H', \boldsymbol{x'}, P'$ and t' are scaled (dimensionless) Hamiltonian, position, momentum, and time, respectively.

The commutation relation of X and P is $[X, P] = i\hbar$. Thus, for the redefined variables

$$[X', P'] = 2K_l * \frac{2K_l}{mw}[X, P] = \frac{4K_l^2}{mw} i\hbar = i\hbar \quad . \quad . \quad . \quad . \quad . \quad (25)$$

$$\hbar = \frac{4\hbar K_l^2}{mw} \quad . \quad . \quad . \quad . \quad . \quad . \quad . \quad . \quad . \quad (26)$$

Here $\hbar$ is the effective Planck's constant [2], [29]. The quantum nature of the system is reflected by the effective Planck´s constant.

The recoil frequency w_R of the applied laser field, on an atom mass m with K_l the photon wave number that makes up a lattice period of $(2K_l)^{-1}$ for the optical potential is.

$$w_R = \frac{\hbar K_l^2}{2m} \quad . \quad . \quad . \quad . \quad . \quad . \quad . \quad . \quad . \quad (27)$$

Using equation 26 and 27, the effective Planck's constant can be related to w_R and w as

$$\hbar = \frac{8w_R}{w} \quad . \quad . \quad . \quad . \quad . \quad . \quad . \quad . \quad . \quad (28)$$

The constant strength of the potential K'

$$K' = \frac{4K_l^2}{mw}\frac{V_0}{w}\tau X_1 = \hbar\frac{\tau V_0 T X_1}{\hbar} = \hbar\Gamma \quad . \quad . \quad . \quad . \quad . \quad . \quad (29)$$

The constant $\Gamma = \frac{\tau V_0 T X_1}{\hbar}$. Here Γ, is the effective kick strength.

With the Hamiltonian earlier defined, the corresponding Schrodinger equation in dimensionless form is.

$$i\hbar\frac{\partial\Psi(x',t')}{\partial t'} = -\frac{\hbar^2}{2}\frac{\partial^2\Psi(x',t')}{\partial x'^2} + K'V'(x',t') \quad . \quad . \quad . \quad . \quad . \quad (30)$$

With $K' = \hbar\Gamma$ and

$$V'(x',t') = (sinx' + \alpha sin2x')\{1 + \frac{1}{\tau\pi}\sum_{k=1}^{\infty}\frac{1}{k}[\sin 2\pi k\tau\, cosk\omega_1 Tt' +$$

$$(1 - \cos 2\pi k\tau)sink\omega_1 Tt']\} \quad . \quad . \quad . \quad . \quad . \quad . \quad . \quad (31)$$

Since $\hbar = 8w_R T$, the value changes as one adjusts the pulsating period T. With $\hbar$ determining the quantum nature of the system, the system dynamic changes with respect to $\hbar$.

3.4 Wave Function and Current

The solution to equation (30), following equation (32) is equation (33)

$$\psi(x',t' + \Delta t') = \widehat{U}(t' + \Delta t', t')\psi(x', t_0') \quad . \quad . \quad . \quad . \quad . \quad (32)$$

$$\psi(x',t' + \Delta t') = \exp\left[-\frac{i\Gamma\Delta t'}{2}\widehat{V'}(x',t' + \Delta t')\right]\exp\left[-\frac{i\hbar\Delta t'}{2}\widehat{D}^2\right]\exp\left[-\frac{i\Gamma\Delta t'}{2}\widehat{V'}(x',t' +$$

$$\Delta t')\right]\psi(x', t_0') \quad . \quad . \quad . \quad . \quad . \quad . \quad . \quad . \quad (33)$$

Where the operator $\widehat{D} = -i\frac{\partial}{\partial x'}$ and $\hat{T} \equiv \frac{\widehat{D}^2}{2}$. Here $\hat{T}$ is the kinetic energy operator. And $\psi(x', t_0')$ is the ground state wave function. This was taken as a homogeneous state given as equation (34)

$$\psi(x', t_0') = 1/\sqrt{2\pi} \quad . \quad . \quad . \quad . \quad . \quad . \quad . \quad . \quad (34)$$

Current

The current from the wave function is computed as

$$J = \langle\widehat{D}\rangle = \left\langle\psi(x',t')\middle|\widehat{D}\middle|\psi(x',t')\right\rangle \quad . \quad . \quad . \quad . \quad . \quad . \quad (35)$$

$$J(x_i', t') = -i\psi^+(x_i', t')[\psi(x_i' + \Delta x', t') - \psi(x_i', t')] \quad . \quad . \quad . \quad (36)$$

Energy

The energy from the wave function is computed as

$$E = \langle\widehat{D}^2\rangle = \left\langle\psi(x',t')\middle|\widehat{D}^2\middle|\psi(x',t')\right\rangle . \quad . \quad . \quad . \quad . \quad . \quad (37)$$

$$E(x_i', t') = -\frac{\psi^+(x_i',t')[\psi(x_i'+\Delta x',t')+\psi(x_i'-\Delta x',t')-2\psi(x_i',t')]}{\Delta x'} \quad . \quad . \quad (38)$$

CHAPTER 4

RESULTS AND DISCUSSION

This chapter contain the results and its discussion for the ratchet cold atom. Python was used in the computation of the Wavefunction dynamics (33), Current (36) and Energy (38). The computation was done for various values of the effective Planck's constant $\hbar$(kbar), Duty cycle τ(ratio of T_1 by T) and Kicked strength Γ(effective potential strength, Gamma). The description of the results of the computation, follows.

4.1 Duty Cycle of Pulse Train

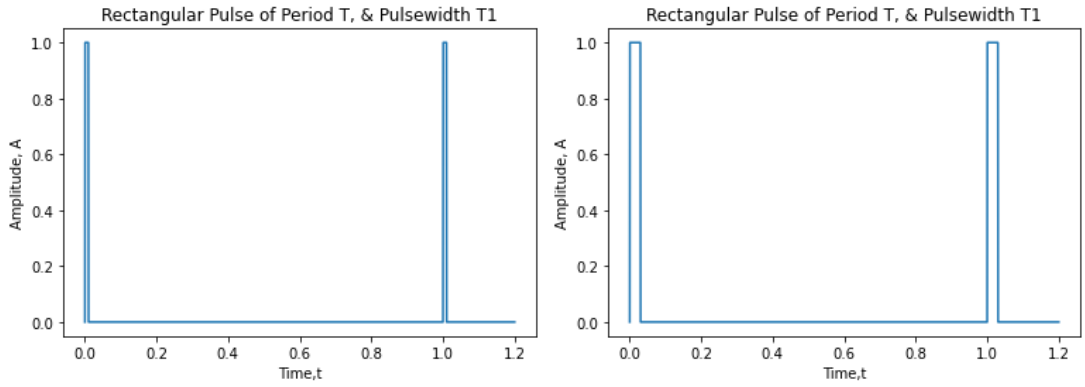

Fig. 4.1: Pulse train of period (T=1), pulse width T_1 and amplitude (A=1) progressing in time t. The pulse train by the left has a duty cycle τ of 0.01 and the one by the right has $\tau = 0.03$.

The pulse trains in Fig. 4.1, were some of the pulse trains that was used in the computation. The pulse train with $\tau = 0.01$ was used to analyse the system in conditions that were earlier computed in delta kicks as it represents a time step closer to the solution of the delta pulse. While pulse trains of $\tau > 0.01$, were used to study the behaviour of the system under the influence of finite pulse.

4.2 Correspondence of Finite Pulse Train Solutions to Delta Kicks at $\tau = 0.01$.

To ensure the validity of results obtained in this work. A study of the results at a condition closer to other works on delta kicks that the results were well established, was compared with this work. Specifically, results of earlier work with delta kicks by Kenfack et al [2], [27], [28] were used. Fig. 4.3, presents one of such results.

The emergence of quantum resonance behaviour at some values of effective Planck's constant $\hbar$ was compared. It should be noted that $\hbar$ is like $\tilde{\hbar}$, and the effective potential strength Γ is influence by τ and is not completely same with the potential strength P from the work of Kenfack et al.

From Fig. 4.2, It can easily be seen that the symmetric nature of emerged resonance between $\hbar/\pi$ equal to 0 to 4 is in harmony with Fig. 4.3. Although at $\hbar/\pi = 4$, in the finite pulse result of Fig. 4.2, shows a resonance point not seen in Fig. 4.3. A possible reason is that the two conditions are not completely same. As such, one should not expect the resonance points to emerged exactly at the same values of $\hbar/\pi$. Since in the regime of $\tau = 0.01$, the finite pulse only approaches the delta pulse case reasonably well. And the $\hbar/\pi = 4$ resonant or a possible pseudo resonant point, grows faster and get to a maximum at some point. This is discussed further in the next section.

It should also be noted that the result of Fig. 4.2 was obtained with 25 kicks while for Fig. 4.3, 200 kicks were used. This is the reason for a large difference in the amplitude of the current between the two. Because the current is proportional to the number of kicks [2].

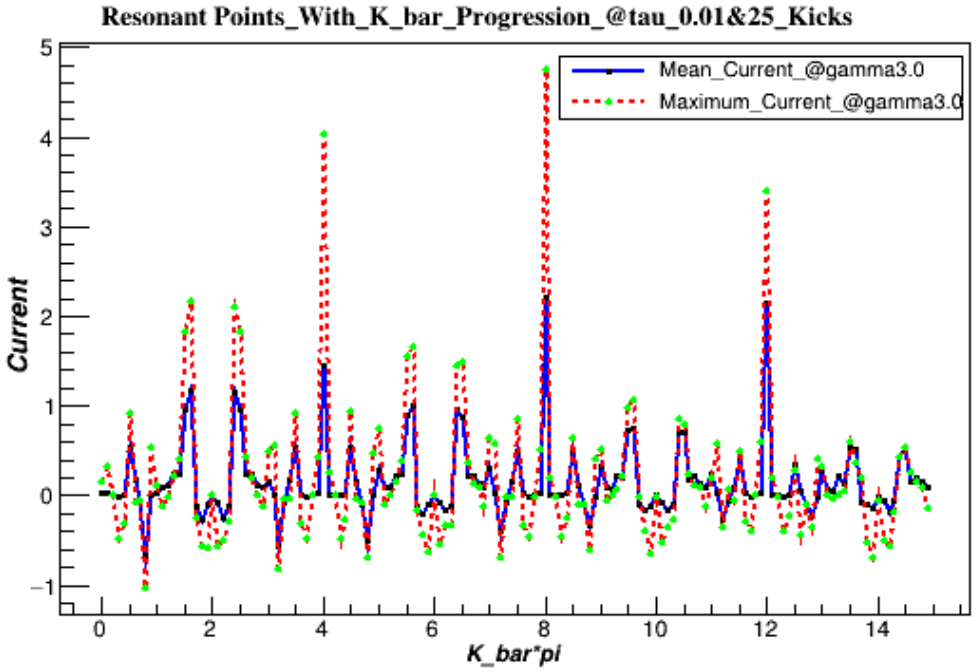

Fig. 4.2. Ratchet current $\langle \widehat{D} \rangle$ as a function of $\hbar/\pi$(K_bar/pi) after 25 kicks, with the potential parameter $\alpha = 0.3$, and effective potential strength $\Gamma = 3.0$(gamma@3.0).

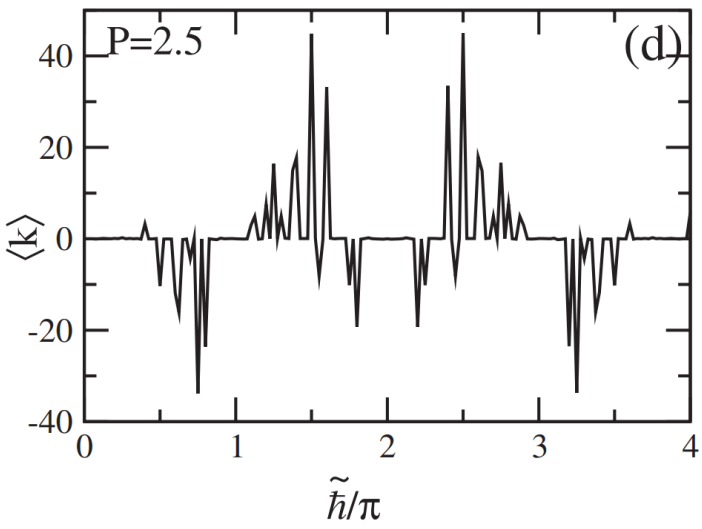

Fig. 4.3: Ratchet current $\langle k \rangle$ as a function of $\tilde{\hbar}/\pi$ after 200 kicks, with the potential parameter $\alpha = 0.3$, and the potential strength P=2.5 indicated in panel.[2]

After running the code for $\hbar/\pi$ values from 0 to 14.9. The behavior of the resonance points emerged became a $\hbar/\pi = 4N$ periodic. This is seen in fig. 2 with $\hbar/\pi = 4{,}8{,}12$ points.

The green and black dots in Fig. 4.2 were the actual values of the maximum and mean current at a specific $\hbar/\pi$. The red dotted and blue continuous lines were only included to help in the visualization of the symmetric nature of the system. And they do not represent the values of the maximum or mean current at points outside the computed dotted green and black currents.

The inclusion of both the maximum and mean currents was a means of validating resonance points from the computations made. When the two reasonably agreed, one picked such point as a resonance point.

4.3 Current and Energy Growth at Resonance points.

The current and energy growth with respect to time were studied. These were done at $\tau = 0.01$ at various gamma and kbar.

At certain values of $\hbar/\pi$, the system experienced a forward directed transport. While for other values, reversal was the case as seen in Fig. 4.4. For the case of the effective

potential strength Γ, for most cases the absolute amplitude of the current is higher for higher value of Γ, except at $\hbar/\pi = 0.8$ where reverse was the case. Therefore, one can´t conclude that, for all cases, higher values of Γ lead to higher absolute current in comparison with the lower Γ's.

For the case of the energy growth. Fig. 4.5 shows that the energy generally increase in accordance with the amplitude of the resonance and higher values of Γ implies higher values of the energy at those resonance points of $\hbar/\pi$. The exception[28] is for $\hbar/\pi = 4$.

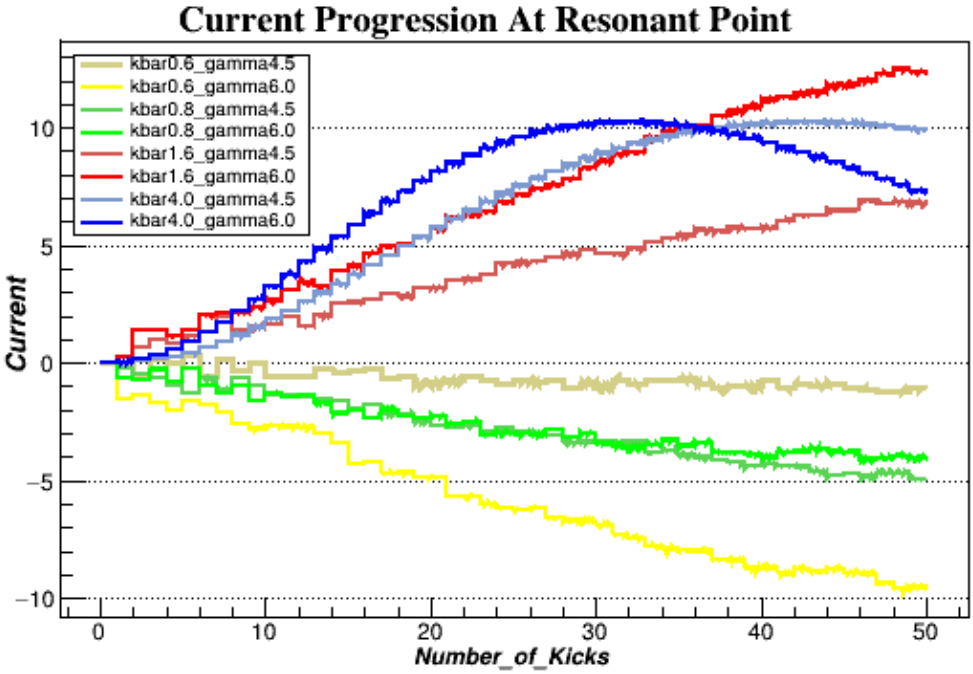

Fig. 4.4: Ratchet current $\langle \widehat{D} \rangle$ as a function of the number of kicks n, at $\tau = 0.01$, with the potential parameter $\alpha = 0.3$. Here the effective potential strength Γ(gamma) and $\hbar/\pi$(kbar) are indicated in the panel.

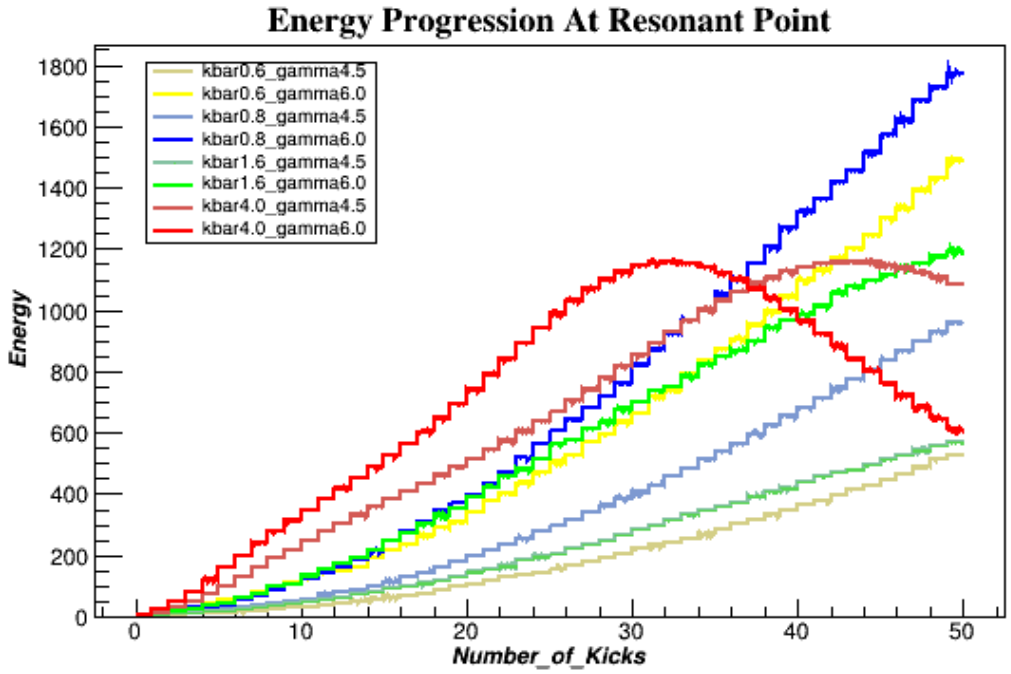

Fig. 4.5: Ratchet Energy $\langle \hat{D}^2 \rangle$ as a function of the Number of Kicks n, at $\tau = 0.01$, with the potential parameter $\alpha = 0.3$. Here the effective potential strength Γ(gamma) and $\hbar/\pi$(kbar) are indicated in the panel.

For the case of $\hbar/\pi = 4$, both the current and energy approach a maximum at certain number of kicks. The maximum was attained faster for the system with higher Γ value. For our case, it occurs approximately at n = 32 and 42 respectively for Γ=6 and 4.5. In both situations, the maximum values of the current and energy are the same, although occurring at different number of kicks.

Under this condition, when the system is kicked before attaining a maximum point, one obtains a resonance point. However, above this number of kicks the value of current begins to decrease. It may be considered as a pseudo resonance point [28]. This may find applications in controlling the system dynamics.

4.4 Finite Pulse Effect with Kbar ($\hbar$)

The cold atom system was computationally set under different values of duty cycle τ. And its response was captured in Fig. 4.6 and 4.7. Fig. 4.6 and 4.7 gives the maximum

and mean current respectively at different $\hbar/\pi$ values. Both graphs would be discussed collectively because the two validate each other on the points where resonance emerged.

The system is subject to 50 kicks at $\Gamma = 4.5$. And was studied at $\tau = 0.010, 0.015, 0.020, 0.025$ and 0.030. These conditions were generally taken because they reflect the general behavior of the system. For example, $\Gamma = 4.5$ was taken because the system shows both forward and current reversal. While the values of τ taken here are within the range of values that shows reasonable results. I.e., the system is not dominated with non-resonance points. Above 0.05, the computation does not show reasonable resonance points.

The results shows that as τ increases, the resonance current amplitude becomes higher at values of $\hbar/\pi$ that are smaller (close to zero) and decreases gradually as $\hbar/\pi$ increases. That is, an inverse relationship. Although, it is not uniform among them. And it somehow breaks or possibly shifted the symmetry point that was seen when $\tau = 0.01$.

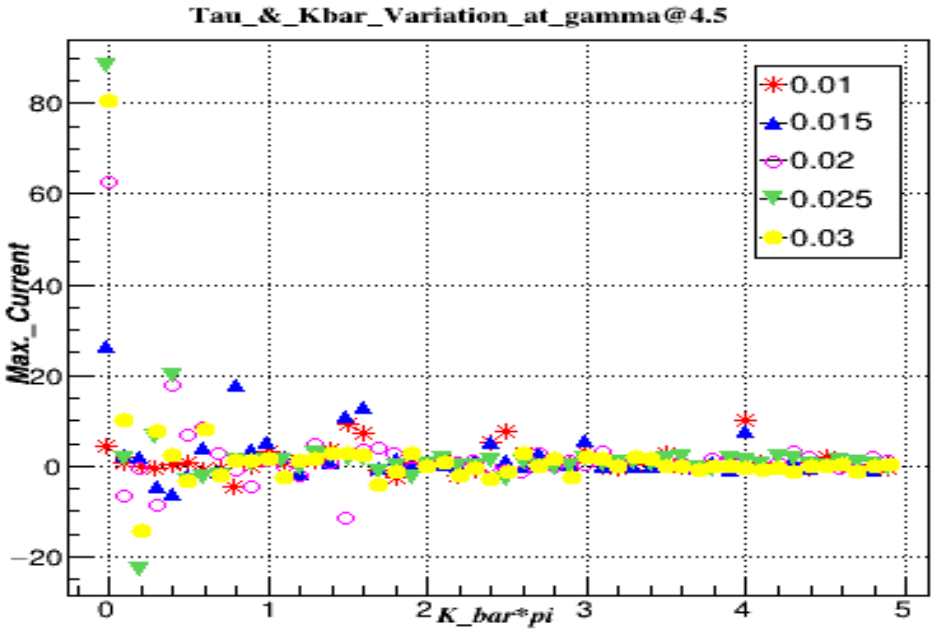

Fig. 4.6: Maximum Current as a function of $\hbar/\pi$(kbar/pi) at $\Gamma = 4.5$, for 50 kicks. And at various value of the duty cycle τ as indicated in the panel.

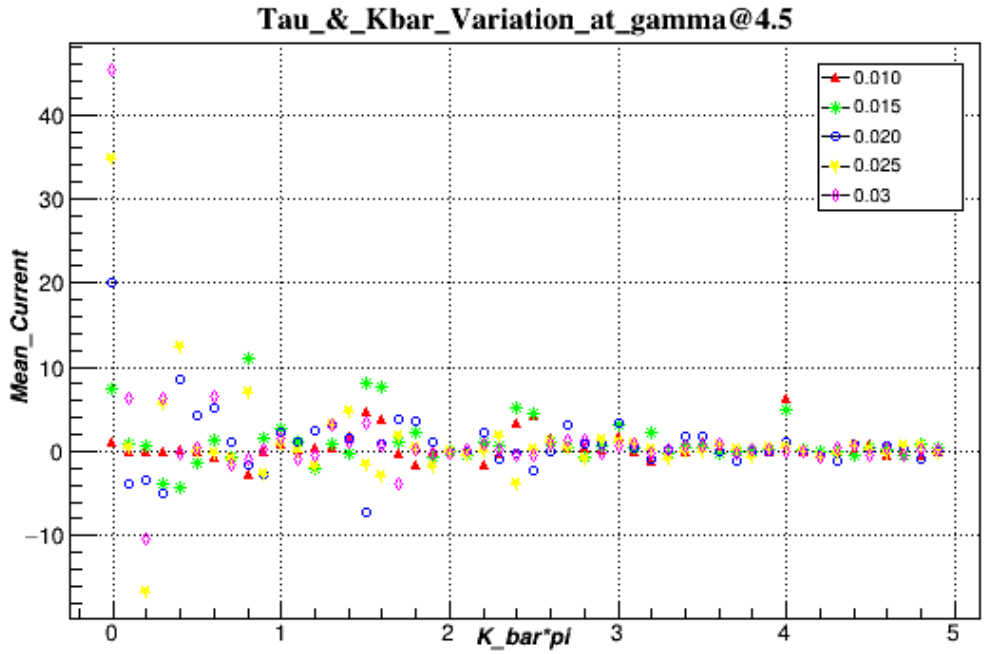

Fig. 4.7: Mean Current as a function of $\hbar/\pi$(kbar/pi) at $\Gamma = 4.5$, for 50 kicks. And at various value of the duty cycle τ as indicated in the panel.

4.5 Finite Pulse Effect with $\hbar = 1.5\pi$ at Various Potential Strength Γ.

The system was set at a resonance point $\hbar = 1.5\pi$ and its behavior with respect to increase in effective potential strength Γ and duty cycle τ was studied.

From Fig. 4.8 and 4.9. One can generally see that the current generally increase slightly rapidly with increase in both the potential strength and the duty cycle.

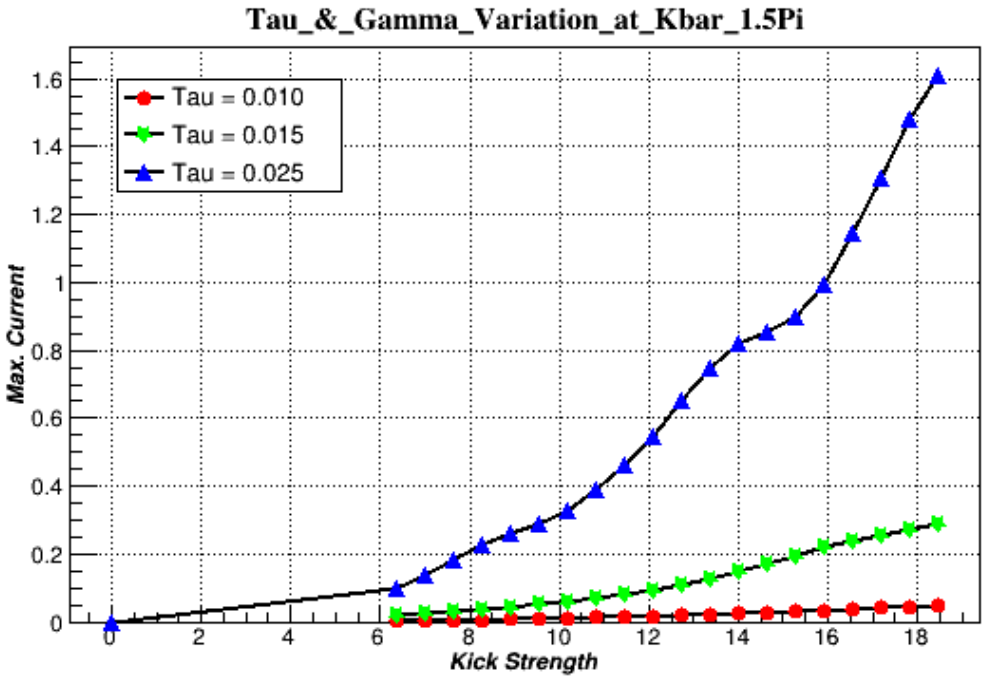

Fig. 4.8: Maximum Current as a function of Γ at (kbar)$\hbar = 1.5\pi$ for 50 kicks. And at various value of the duty cycle τ as indicated in the panel.

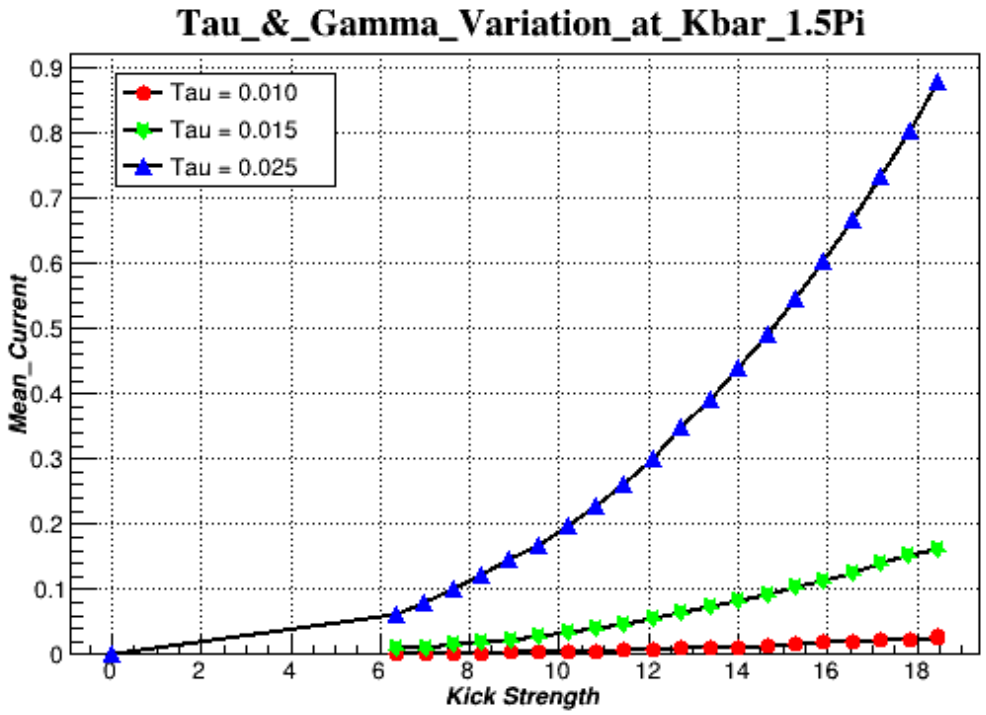

Fig. 4.9: Mean Current as a function of Γ at (kbar)$\hbar = 1.5\pi$ for 50 kicks. And at various value of the duty cycle τ as indicated in the panel.

4.6 Finite Pulse Effect for Various Potential Strength Γ and $\hbar/\pi$(kbar/pi) Variation at $\tau = 0.01$

Since the effective kicked strength in the finite pulse definition is not the same as that for infinite pulse, the results of the resonance points at different kbar and gamma were computed and presented in fig. 10 and 11.

One can easily observe a gradual transition from lower order to higher order resonance as Γ increases. It is an expected result based on the infinite pulse analysis [2].

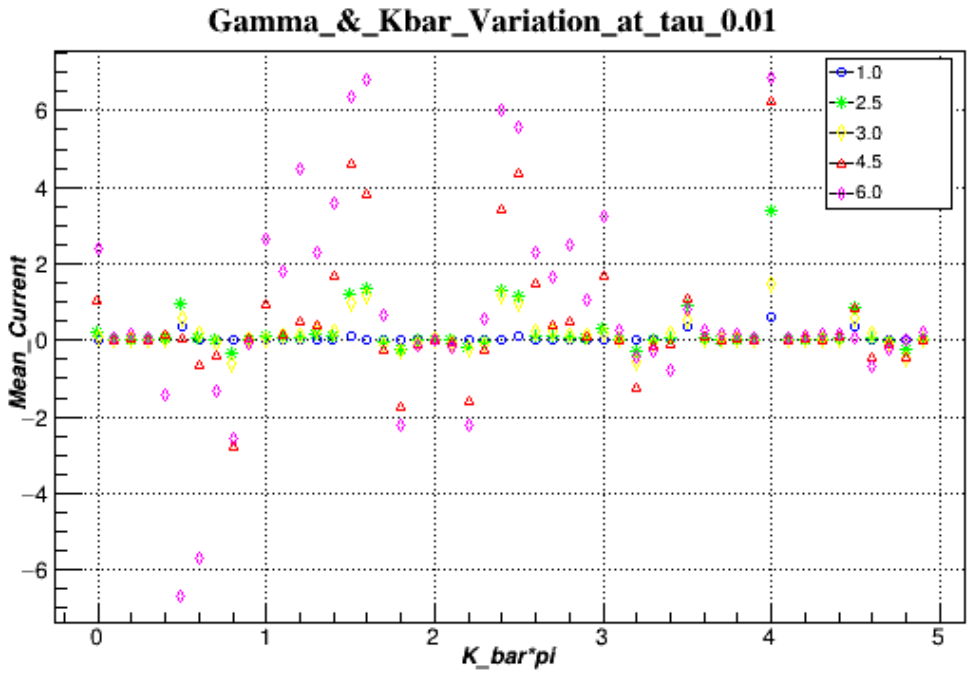

Fig. 4.10: Mean current as a function of $\hbar/\pi$(K_bar/pi) after 50 kicks, with the potential parameter $\alpha = 0.3$, and with various effective potential strength Γ as seen in the panel. And at $\tau = 0.01$

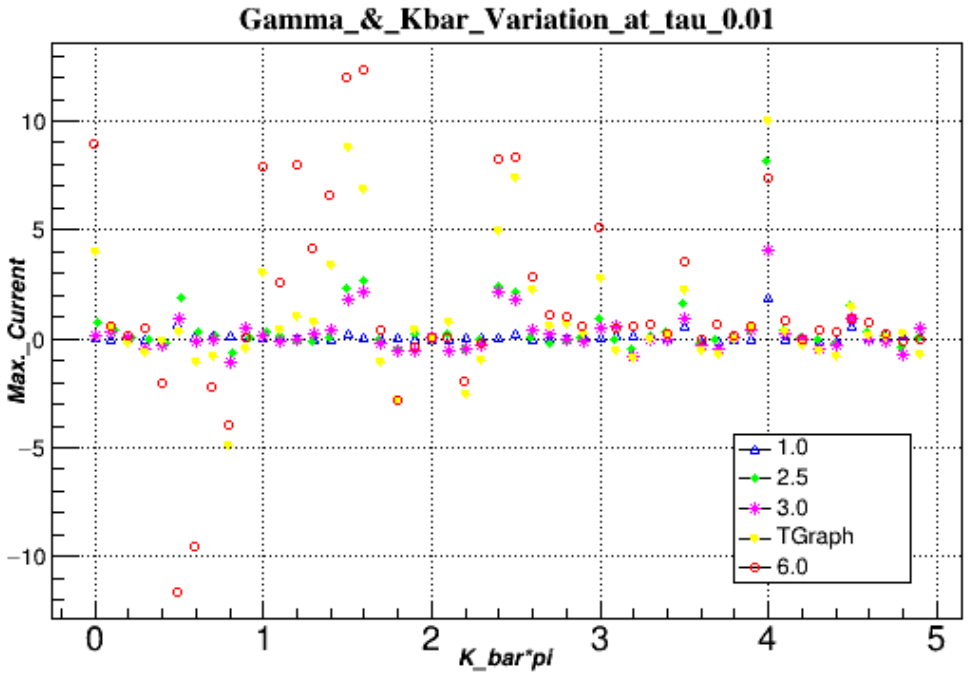

Fig. 4.11: Max current as a function of $\hbar/\pi$(K_bar/pi) after 50 kicks, with the potential parameter $\alpha = 0.3$, and with various effective potential strength Γ as seen in the panel. And at $\tau = 0.01$

CHAPTER 5

CONCLUSION AND OUTLOOK

This chapter present some conclusion that were obtained from the results earlier presented in the previous chapter. It further gives some areas of interest that can possibly be explore in the next stage of this topic.

5.1 Conclusion

Motivated to obtain a more realistic flashing ratchet directed transport result. The ratchet effect of cold atoms was studied by developing and implementing a computational code that include the finite pulse behaviour of an optical laser potential.

This study successfully gives results that approaches those of delta pulses at $\tau = 0.01$. And some extend, justify the developed approached.

It was realized that τ influence the amplitude of the resonance current. With increase in τ within the studied region, the amplitude of the pulses decreases as kbar increases.

And it was also shown that at a fixed resonance point (kbar/pi =1.5), the ratchet current reasonably increases rapidly with increase of both τ and the kicked strength gamma.

5.2 Outlook

Some suggestions for future research are:

The code should be further explored outside the domain that the results of this work was centred on. For example, one can consider the behaviour of the system at a very high values of duty cycle with very fine adjustment and varying the various parameters. There may be some regions where resonances exit but have not been observed because they were not explored.

The code should be extended into a 2D map, to have a clearer and extensive picture of the behaviour of the system subject to finite pulse.

REFERENCE

[1] M. Sadgrove, M. Horikoshi, T. Sekimura, and K. Nakagawa, "Rectified momentum transport for a kicked Bose-Einstein condensate," *Phys. Rev. Lett.*, vol. 99, no. 4, pp. 1–4, 2007, doi: 10.1103/PhysRevLett.99.043002.

[2] A. Kenfack, J. Gong, and A. K. Pattanayak, "Controlling the ratchet effect for cold atoms," *Phys. Rev. Lett.*, vol. 100, no. 4, 2008, doi: 10.1103/PhysRevLett.100.044104.

[3] R. Gommers, S. Bergamini, and F. Renzoni, "Dissipation-induced symmetry breaking in a driven optical lattice," *Phys. Rev. Lett.*, vol. 95, no. 7, pp. 1–5, 2005, doi: 10.1103/PhysRevLett.95.073003.

[4] A. Kenfack, "Introduction to the Theory of Laser Matter Interaction," 2020.

[5] R. Gommers, "Symmetry and Transport in Cold Atom Ratchets Symmetry and Transport in Cold Atom Ratchets," no. June, 2007.

[6] C. Hainaut *et al.*, "Ratchet effect in the quantum kicked rotor and its destruction by dynamical localization," *Phys. Rev. A*, vol. 97, no. 6, pp. 1–5, 2018, doi: 10.1103/PhysRevA.97.061601.

[7] V. Lebedev and F. Renzoni, "Two-dimensional rocking ratchet for cold atoms," *Phys. Rev. A - At. Mol. Opt. Phys.*, vol. 80, no. 2, pp. 1–5, 2009, doi: 10.1103/PhysRevA.80.023422.

[8] D. Medhat Mohamed Abdel Maksoud, "Study of New Miniaturized Microwave Devices based on Ratchet Effect in an Environment of Asymmetric Nano-Scatterers," Institut National Polytechnique de Toulouse - INPT, 2012.

[9] A. K. Mukhopadhyay and P. Schmelcher, "Multiple current reversals using superimposed driven lattices," *Appl. Sci.*, vol. 10, no. 4, pp. 38–46, 2020, doi: 10.3390/app10041357.

[10] V. Milner, D. A. Steck, W. H. Oskay, and M. G. Raizen, "Recovery of classically chaotic behavior in a noise-driven quantum system," *Phys. Rev. E - Stat. Physics, Plasmas, Fluids, Relat. Interdiscip. Top.*, vol. 61, no. 6 B, pp. 7223–7226, 2000, doi: 10.1103/PhysRevE.61.7223.

[11] S. Denisov, Y. Zolotaryuk, S. Flach, and O. Yevtushenko, "Vortex and translational currents due to broken time-space symmetries," *Phys. Rev. Lett.*, vol. 100, no. 22, pp. 4–7, 2008, doi: 10.1103/PhysRevLett.100.224102.

[12] J. Casado-Pascual, D. Cubero, and F. Renzoni, "Universal asymptotic behavior in nonlinear systems driven by a two-frequency forcing," *Phys. Rev. E - Stat. Nonlinear, Soft Matter Phys.*, vol. 88, no. 6, 2013, doi: 10.1103/PhysRevE.88.062919.

[13] S. Edris, "The Ratchet Effect with cold atoms," University College London, 2019.

[14] Richard Phillips Feynman, "The Feynman Lectures on Physics Vol. I Ch. 46: Ratchet and pawl." https://www.feynmanlectures.caltech.edu/I_46.html (accessed Mar. 28, 2021).

[15] T. Y. Tsong, "Na,K-ATPase as a Brownian Motor: Electric Field-Induced Conformational Fluctuation Leads to Uphill Pumping of Cation in the Absence of ATP," 2002.

[16] M. O. Magnasco, "Forced thermal ratchets," *Phys. Rev. Lett.*, vol. 71, no. 10, pp. 1477–1481, 1993, doi: 10.1103/PhysRevLett.71.1477.

[17] J.-F. Chauwin, A. Ajdari, and J. Prost, "Force-Free Motion in Asymmetric Structures: A

Mechanism without Diffusive Steps," *Europhys. Lett.*, vol. 27, no. 6, pp. 421–426, Aug. 1994, doi: 10.1209/0295-5075/27/6/002.

[18] J. Rousselet, L. Salome, A. Ajdari, and J. Prostt, "Directional motion of brownian particles induced by a periodic asymmetric potential," *Nature*, vol. 370, no. 6489, pp. 446–448, 1994, doi: 10.1038/370446a0.

[19] L. P. Faucheux, L. S. Bourdieu, P. D. Kaplan, and A. J. Libchaber, "Optical thermal ratchet," *Phys. Rev. Lett.*, vol. 74, no. 9, pp. 1504–1507, 1995, doi: 10.1103/PhysRevLett.74.1504.

[20] A. Van Oudenaarden and S. G. Boxer, "Brownian ratchets: Molecular separations in lipid bilayers supported on patterned arrays," *Science (80-.).*, vol. 285, no. 5430, pp. 1046–1048, 1999, doi: 10.1126/science.285.5430.1046.

[21] H. Linke, "Experimental Tunneling Ratchets," vol. 2314, no. 1999, 2008, doi: 10.1126/science.286.5448.2314.

[22] C. S. Lee, B. Jankó, I. Derényl, and A. L. Barabási, "Reducing vortex density in superconductors using the 'ratchet effect,'" *Nature*, vol. 400, no. 6742, pp. 337–340, 1999, doi: 10.1038/22485.

[23] V. Serreli, C. Lee, E. R. Kay, and D. A. Leigh, "A Molecular Information Ratchet," *Nature*, vol. 527, pp. 1–6, 2007, [Online]. Available: papers2://publication/uuid/9CFDBBB1-0369-40B1-8B02-9B0E728CA696.

[24] S. Yukawa, M. Kikuchi, G. Tatara, and H. Matsukawa, "Quantum Ratchets," *J. Phys. Soc. Japan*, vol. 66, no. 10, pp. 2953–2956, 1997, doi: 10.1143/JPSJ.66.2953.

[25] C. Jarzynski, "Nonequilibrium equality for free energy differences," *Phys. Rev. Lett.*, vol. 78, no. 14, pp. 2690–2693, 1997, doi: 10.1103/PhysRevLett.78.2690.

[26] R. Gommers, S. Denisov, and F. Renzoni, "Quasiperiodically driven ratchets for cold atoms," *Phys. Rev. Lett.*, vol. 96, no. 24, 2006, doi: 10.1103/PhysRevLett.96.240604.

[27] E. Lundh and M. Wallin, "Ratchet effect for cold atoms in an optical lattice," *Phys. Rev. Lett.*, vol. 94, no. 11, 2005, doi: 10.1103/PhysRevLett.94.110603.

[28] L. Chen *et al.*, "Quantum ratchet effect in a time non-uniform double-kicked model," *Int. J. Mod. Phys. B*, vol. 31, no. 16–19, pp. 1–5, 2017, doi: 10.1142/S0217979217440635.

[29] P. H. Jones, M. Goonasekera, H. E. Saunders-Singer, and D. R. Meacher, "Shifting the boundaries: Pulse-shape effects in the atom-optics kicked rotor," *Europhys. Lett.*, vol. 67, no. 6, pp. 928–933, 2004, doi: 10.1209/epl/i2004-10198-1.

[30] C. Grossert, M. Leder, S. Denisov, P. Hänggi, and M. Weitz, "Experimental control of transport resonances in a coherent quantum rocking ratchet," *Nat. Commun.*, vol. 7, 2016, doi: 10.1038/ncomms10440.

[31] C. M. Dion, A. Hashemloo, and G. Rahali, "Program for quantum wave-packet dynamics with time-dependent potentials," *Comput. Phys. Commun.*, vol. 185, no. 1, pp. 407–414, 2014, doi: 10.1016/j.cpc.2013.09.012.

[32] Y. I. Salamin, S. X. Hu, K. Z. Hatsagortsyan, and C. H. Keitel, "Relativistic high-power laser-matter interactions," *Phys. Rep.*, vol. 427, no. 2–3, pp. 41–155, 2006, doi: 10.1016/j.physrep.2006.01.002.

[33] J. Javanainen and J. Ruostekoski, "Split-step Fourier methods for the Gross-Pitaevskii equation," no. 4, pp. 4–6, 2004, doi: 10.1088/0305-4470/39/12/L02.

[34] F. Blumenthal and H. Bauke, "A stability analysis of a real space split operator method

for the Klein-Gordon equation," *J. Comput. Phys.*, vol. 231, no. 2, pp. 454–464, 2012.

[35] G. R. Mocken and C. H. Keitel, "FFT-split-operator code for solving the Dirac equation in 2+1 dimensions," *Comput. Phys. Commun.*, vol. 178, no. 11, pp. 868–882, 2008, doi: 10.1016/j.cpc.2008.01.042.

[36] "Generating Pulses." https://www.ge.infn.it/~didomizi/documenti/daq/Ni_Docs/software/daqhelp.chm/generating_pulses.html (accessed Mar. 29, 2021).